Nonadiabatic Ab Initio Multichannel Quantum Defect Theory Applied to Absolute Experimental Absorption Intensities in H_2[†]

M. Glass-Maujean[‡] and Ch. Jungen*[,§,⊥]

Laboratoire de Physique Moléculaire pour l'Atmosphère et l'Astrophysique, Université Pierre et Marie Curie, 4 place Jussieu, 75252 Paris Cedex 05, France, Laboratoire Aimé Cotton du CNRS, Bâtiment 505, Université de Paris-Sud, F-91405 Orsay, France, and Department of Physics and Astronomy, University College London, London WC1E 6BT, United Kingdom

Received: March 30, 2009; Revised Manuscript Received: May 25, 2009

The positions and intensities of the $Q(N)$ ($N = 1-4$) $X^1\Sigma_g^+ \rightarrow np\pi^1\Pi_u^-$ ($n = 2$ to ~ 30) absorption transitions of H_2 have been calculated by multichannel quantum defect theory. The computations are based on the quantum chemical ab initio clamped nuclei potential curves and absorption dipole transition moments for $n = 2-4$ of Wolniewicz and Staszewska (*J. Mol. Spectrosc.* **2003**, *220*, 45). The resulting Einstein spontaneous Einstein *A* coefficients are in good agreement with those derived from the absolute intensity measurements of Glass-Maujean et al. (*Mol. Phys.* **2007**, *105*, 1535). The results reveal widespread vibronic intensity perturbations in the $Q(N)$ Rydberg series, whereas the line frequencies are comparatively little affected by nonadiabatic effects.

1. Introduction

Multichannel quantum defect theory (MQDT) combined with the frame transformation concept is perhaps the most successful theoretical approach capable of treating electronically excited molecular systems beyond the Born−Oppenheimer approximation.[1−4] It surpasses the traditional coupled equations approach in that it is not restricted to just a few excited states which have to be added to the treatment one by one but instead handles whole families of excited states (Rydberg series) up to the ionization thresholds and beyond. Furthermore, using the powerful concept of frame transformations, MQDT bypasses the evaluation of the electronic coupling matrix elements, which require the knowledge of numerical ab initio electronic wave functions. A quantitative comparison of the two approaches may be made by referring to two papers which appeared more than 10 years ago,[5,6] where each theory was applied to the same vibronic problem.

Numerous applications of MQDT to molecular spectroscopic problems have been published during the last decades, progressing from rotationally resolved absorption,[4,7] emission,[8] or multiphoton ionization spectroscopy and dynamics[9,10] to hyperfine resolved millimeter wave and photoionization spectroscopy.[11−13] However, to our knowledge, no quantitative MQDT study of molecular line intensities of any molecule has been made so far in a situation where absolute measured line intensities were available for comparison.

In this paper, we present a fully ab initio calculation of the line positions and intensities of the $Q(N)$ ($N = 1-4$) absorption transitions in molecular hydrogen H_2, based on MQDT. We extract the quantum defects and channel dipole transition moments from the latest ab initio calculations of Wolniewicz and collaborators[14−16] and use them in the framework of the nonadiabatic frame transformation-MQDT. We obtain overall good agreement with the recent synchrotron-based absolute intensity measurements of Glass-Maujean et al.[17] It is well-known that the energy positions of the excited levels of H_2 of $^1\Pi_u^-$ symmetry (which are the upper states reached by the Q transitions) are only little affected by vibronic interactions. By contrast, the intensities of the Q transitions are surprisingly strongly perturbed by the $^1\Pi u - \sim {}^1\Pi_u^-$ vibronic interactions in many instances, even when the line positions are apparently unperturbed. This fact had been established experimentally in ref 17 and is confirmed by the present calculations.

2. Determination of Quantum Defects and Channel Transition Moments from Quantum Chemical Data

We use quantum defect theory in its simplest form by disregarding channel interactions between singly excited and doubly (core) excited Rydberg channels. In other words, we assume that the manifold of the $^1\Pi_u$ excited states of H_2 represent a single unperturbed $np\pi$ Rydberg series converging to the $X^+\ ^2\Sigma_g^+$ ground state of H_2^+. Correlation between the excited electron and the ion core electron are included in an effective manner in the quantum defects because we extract the latter from highly accurate theoretical clamped nuclei (Born−Oppenheimer) potential energy curves[14,16] in which electron correlation has been fully accounted for. We use the familiar one-channel Rydberg equation

$$U_{np\pi}(R) = U^+(R) - \frac{1}{2[n - \mu_{np\pi}(R)]^2} \qquad (1)$$

written here in atomic energy units in order to extract the quantum defects for $^1\Pi_u$ symmetry. $U_{np\pi}(R)$ is the clamped nuclei curve for the $np\pi$ Rydberg state and $U^+(R)$ is the corresponding curve for the ion ground state, $X^+\ ^2\Sigma_g^+$. We used the data for $n = 2$ (C state), 3 (D state), and 4 (D′ state) from ref 14 (see Figure 1), which yield the quantum defect curves for $n = 2$, 3, and 4. The set of clamped nuclei quantum defect

[†] Part of the "Robert W. Field Festschrift".
* To whom correspondence should be addressed.
[‡] Université Pierre et Marie Curie.
[§] Université de Paris-Sud.
[⊥] University College London.

10.1021/jp902846c CCC: $40.75
Published on Web 06/23/2009

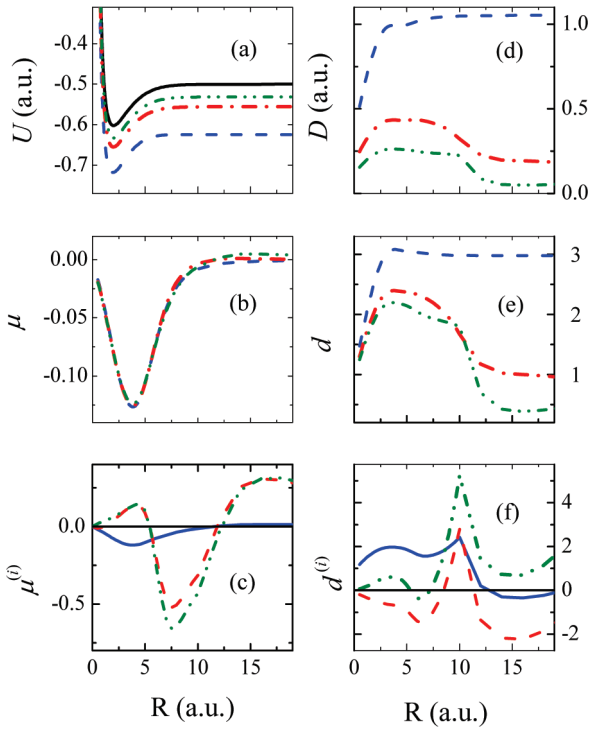

Figure 1. Reduction of quantum chemical data to channel parameters adapted to MQDT (H_2, $^1\Pi_u$). (a) Ab initio potential energy curves $U_{np\pi}(R)$; $n = 2$ (dashed line), 3 (dot−dashed line), 4 (dot−dot−dashed line), and $U^+(R)$ (ion, full line). (b) Quantum defects $\mu_{np\pi}$ ($n = 2-4$) (eq 1, same symbols as those for the top panels). (c) Quantum defect functions $\mu^{(0)}(R)$ (full line), $\mu^{(1)}(R)$ (dashed line), and $0.1 \times \mu^{(2)}(R)$ (dot−dot−dashed line) (eq 2). (d) Ab initio dipole transition moments $D_{X\to np\pi}(R)$ for $n = 2-4$ (same symbols as thosein (a)). (e) Energy-normalized transition moments obtained after multiplication by the density of states (same symbols as those in (d)). (f) Dipole transition functions $d^{(0)}(R)$, $0.1 \times d^{(1)}(R)$, and $0.01 \times d^{(2)}(R)$ (same symbols as those in (c); eq 3).

curves thus obtained is subsequently represented by an energy-dependent polynomial of the form

$$\mu(\epsilon, R) = \mu^{(0)}(R) + [\epsilon(R)]\mu^{(1)}(R) + \frac{1}{2}[\epsilon(R)]^2\mu^{(2)}(R) + \frac{m}{M}\mu^{\text{specific}}(R) \quad (2)$$

where $\epsilon(R) = U_{np\pi}(R) - U^+(R)$ is the binding energy of the Rydberg electron in the field of the core with the nuclei kept fixed at a distance R. (The fourth term on the rhs of eq 2 is discussed below.) The process of reducing the three available ab initio curves $U_{np\pi}(R)$ to the three functions $\mu^{(0)}(R)$, $\mu^{(1)}(R)$, and $\mu^{(2)}(R)$ is illustrated in Figure 1a−c. Note that the functions $\mu^{(0)}(R)$, $\mu^{(1)}(R)$, and $\mu^{(2)}(R)$ allow us to recover the potential energy curves for $n = 2-4$ exactly (because for each R, three values have been represented in terms of three parameters) by means of eqs 1 and 2, but we also can predict all of the higher curves with $n > 4$. The reliability of this extrapolation (within reasonable limits) is suggested by the fact that the three quantum defect curves in Figure 1b nearly coincide.

The last term in eq 2 corresponds to the "specific" mass effect (mass polarization term) arising from the cross term $H_3' = -(m/4M)\nabla_1\nabla_2$ in the molecular Hamiltonian (where m is the electron mass and M is the nuclear reduced mass). This term couples the Rydberg and the core electrons and, as shown in ref 4, contributes a small mass-dependent correction to the quantum defect. In quantum chemical computations, the same term arises as part of the adiabatic corrections but unfortunately is rarely given separately when these are evaluated. Following ref 4, we take it here independent of R, and energy. We use the value $\mu^{\text{specific}} = -0.16$ for the $np\pi\,^1\Pi_u$ channel.

A similar procedure is applied to the ab initio dipole transition moments from refs 14 and 16. We first reduce the values $D_{X\to np\pi}(R)$ (Figure 1d) to energy-normalized transition moments $d_{X\to np\pi}(R)$ by multiplying by the square root of the density of states $d\nu/d\epsilon = (n - \mu_{np\pi})^{3/2}$ (in au, where $\nu = n - \mu = (-2\epsilon)^{-1/2}$) (Figure 1e). It may be seen that the energy-normalized moments d, while exhibiting less energy dependence than the moments D shown at the top, are by no means as constant as their quantum defect counterparts represented in Figure 1b. The reasons for this will be discussed in section 6 below. We note on the other hand that the photon absorption from the ground state effectively takes place in a small region centered around the equilibrium position near 1.4 a_0, where the energy dependence of the d's is relatively mild. We finally represent these reduced moments for each R by an expression analogous to eq 2

$$d(\epsilon, R) = d^{(0)}(R) + [\epsilon(R)]d^{(1)}(R) + \frac{1}{2}[\epsilon(R)]^2 d^{(2)}(R) \quad (3)$$

The resulting channel dipole transition functions $d^{(0)}(R)$, $d^{(1)}(R)$, and $d^{(2)}(R)$ for excitation from the ground state to the pπ Rydberg channel are shown in Figure 1f. In agreement with what has just been said, the quantities $d^{(1)}$ and $d^{(2)}$ are seen to be rather small in the region around $R_e = 1.4\ a_0$.

3. Vibronic MQDT Calculations

3.1. Theoretical Aspects. The frame transformation method has been implemented using well-documented MQDT technology.[2,5,18] In the case of the $Q(N)$ spectral lines and when hyperfine effects are neglected, the upper states are of pure $^1\Pi_u^-$ symmetry, and therefore, there are no rotational channel couplings, with the result that only the vibrational frame transformation has to be applied. This is done by evaluating integrals of the type

$$\mu^{(q,N,d)}_{v^+N^+,v^{+'}N^{+'}} = \int \chi_{v^+N^+}(R)\mu^{(q)}(R)\chi_{v^{+'}N^{+'}}(R)\mathrm{d}R \quad (4)$$

where $N^+ = N^{+'}$ in the present case. The $\mu^{(q)}$, with index $q = 0-2$, are the quantum defect functions of eq 2, and $\chi_{v^+N^+}(R)$ are the vibrational eigenfunctions of H_2^+ in the vibration−rotation level v^+, N^+ of the electronic ground state. The superscript N ($= N^+ = N^{+'}$) refers to the total angular momentum of the molecule exclusive of spins, while d refers to Kronig's symmetry label, designating levels that have a total parity of $-(-1)^N$.

The energy-dependent vibronic quantum defect matrix is expressed in terms of the vibrational integrals eq 4 as

$$\mu^{(N,d)}_{v^+N^+,v^{+'}N^{+'}}(E) = \mu^{(0,N,d)}_{v^+N^+,v^{+'}N^{+'}} + \bar{\epsilon}\mu^{(1,N,d)}_{v^+N^+,v^{+'}N^{+'}} + \frac{1}{2}\bar{\epsilon}^2\mu^{(2,N,d)}_{v^+N^+,v^{+'}N^{+'}} \quad (5)$$

where again $N^+ = N^{+'} = N$ and where the reference energy $\bar{\epsilon}(E)$ is taken as the mean of the channel energies for each pair of coupled channels

$$\bar{\epsilon} \equiv \bar{\epsilon}_{v^+N^+,v^{+\prime}N^{+\prime}}(E) = \frac{1}{2}[(E - E^+_{v^+N^+}) + (E - E^+_{v^{+\prime}N^{+\prime}})] \tag{6}$$

(The mass polarization term involving μ^{specific}, which appears in eq 2, is assumed here to be included with $\mu^{(0,N,d)}_{v^+N^+,v^{+\prime}N^{+\prime}}$).

The vibronic quantum defect matrix $\mu^{(N,d)}_{v^+N^+,v^{+\prime}N^{+\prime}}(E)$ of eq 5 thus evaluated must now be converted into vibronic matrices $\mathcal{J}$ and $\mathcal{C}$, defined such that the vibronic reaction matrix **K** is given by $\mathbf{K} = \mathcal{J}\mathcal{C}^{-1}$. These matrices are defined as $\mathcal{J} = \mathbf{U}\sin\pi\mu_\alpha\mathbf{U}^{\text{tr}}$ (with sin replaced by cos or tan in the case of $\mathcal{C}$ and **K**, respectively),[4] where **U** is the eigenvector matrix of **K** and μ_α are the associated eigenquantum defects. The conversion is done by employing the procedures described in refs 5 and 19. The vibronic level energies are then calculated using the well-known MQDT quantization condition

$$\sum_k [\cos(\pi\nu_j)\mathcal{J}_{jk} + \sin(\pi\nu_j)\mathcal{C}_{jk}]B_k = 0 \tag{7}$$

for each channel j. The $\nu_j(E) = [-2(E - E^+_j)]^{-1/2}$ are the channel effective quantum numbers and B_k are the channel mixing coefficients. The indices j and k run over all vibrational channels v^+N^+ specified above. Once an energy $E = E_n$ has been found such that eq 7 is satisfied for all j, the level energy, taken relative to the ionization potential and in wavenumber units, becomes

$$[(E_n - E^+_{v^+=0,N^+=0})/hc] = -\frac{\mathcal{R}_{\text{H}_2}}{[\nu_{v^+=0,N^+=0}(E_n)]^2} \tag{8}$$

where $\mathcal{R}_{\text{H}_2}$ is the mass-corrected Rydberg constant and E_n is the level energy in joules. Note that the use of the mass-corrected Rydberg constant instead of $\mathcal{R}_\infty$ is equivalent to including the term $-(m/2M)\nabla^2_{\text{I}}$ of the molecular Hamiltonian, which, in the standard approach, is part of the adiabatic correction.[4]

An analogous procedure is applied to the transition dipole moments eq 3. These are used to calculate vibronic channel dipole transition matrix elements

$$d^{(q,N,d)}_{v^+N^+,v''N''} = \int \chi_{v^+N^+}(R)d^{(q)}(R)\chi_{v''N''}(R)\text{d}R \tag{9}$$

where $\chi_{v''N''}(R)$ is the vibrational wave function in the ground-state initial level, which has Kronig symmetry c, and where $N = N'' = N^+$ since we are dealing with Q-transitions here. The quantities $d^{(q,N,d)}_{v^+N^+,v''N''}$, $q = 0-2$, evaluated with the help of eq 9, are used to construct a set of energy-dependent vibronic transition moments in analogy with eq 5

$$d^{(N,d)}_{v^+N^+v''N''}(E) = d^{(0,N,d)}_{v^+N^+,v''N''} + \bar{\epsilon}d^{(1,N,d)}_{v^+N^+,v''N''} + \frac{1}{2}\bar{\epsilon}^2 d^{(2,N,d)}_{v^+N^+,v''N''} \tag{10}$$

The reference energy $\bar{\epsilon}(E)$ is here taken as

$$\bar{\epsilon} \equiv \bar{\epsilon}_{v^+N^+}(E) = [(E - E^+_{v^+N^+})] \tag{11}$$

The effective transition moment to the bound Rydberg state n is finally given by the following superposition of channel amplitudes:

$$D_n = \frac{1}{\mathcal{N}}\sum_k d_{k,k''}(E_n)B_k(E_n) \tag{12}$$

where B_k are the channel mixing coefficients obtained by solving eq 7 and where, again, k stands for the ionization channels v^+N^+ and k'' stands for $v''N''$. $\mathcal{N}$ is the overall normalization factor of the bound state wave function.

The normalization integral, $\mathcal{N}^2$, for a bound Rydberg state satisfying the quantization condition eq 7 reads

$$\mathcal{N}^2 = \frac{1}{\pi}\sum_j \frac{\partial\beta_j}{\partial\epsilon_j}[\sum_k(\cos\beta_j\mathcal{C}_{jk} - \sin\beta_j\mathcal{J}_{jk})B_k]^2 + \frac{1}{\pi}\sum_j[\sum_k(\cos\beta_j\mathcal{C}_{jk} - \sin\beta_j\mathcal{J}_{jk})B_k] \times \left[\sum_k\left(\sin\beta_j\frac{\partial\mathcal{C}_{jk}}{\partial\epsilon_j} + \cos\beta_j\frac{\partial\mathcal{J}_{jk}}{\partial\epsilon_j}\right)B_k\right] \tag{13}$$

where the indices j and k run over all vibrational channels v^+ in the present application, and $\beta_j = \pi(\nu_j - l)$. $\partial\beta_j/\partial\epsilon_j = \pi\nu_j^3$ (in au) is the well-known Rydberg scaling factor. Equation 13 is a straightforward generalization of expressions given in Appendix A of ref 20.

The transition moment D_n for each particular spectral line is finally converted into the Einstein coefficient A for the transition by means of the relation

$$A_{n\rightarrow v''N''} = \frac{4}{3}\frac{mc^2}{\hbar}\alpha^5\left(\frac{E_n - E_{v''N''}}{2\mathcal{R}hc}\right)^3\left|\frac{D_n}{ea_0}\right|^2 = 2.142\times10^{10}\left(\frac{E_n - E_{v''N''}}{2\mathcal{R}hc}\right)^3\left|\frac{D_n}{ea_0}\right|^2 \text{ s}^{-1} \tag{14}$$

Here, α is the fine structure constant. The transition energy $E_n - E_{v''N''}$ is in joules, and the transition moment D_n is in coulomb·meters. The brackets (. . .) and |. . .| contain, respectively, the transition energy and the dipole transition moment in atomic units.

3.2. Numerical Details. The vibration−rotation wave functions $\chi_{v^+N^+}$ have been evaluated in the adiabatic approximation using the ion ground-state potential energy curve of Wind[21] and the adiabatic correction terms of Bishop and Wetmore.[22] The corresponding ion levels $E^+_{v^+,N^+}$ are those of Wolniewicz and Orlikowski,[23] evaluated including the nonadiabatic and relativistic interactions in addition to the adiabatic corrections. These ion level energies do not include the hyperfine interactions, but their accuracy is largely sufficient in the present context. We used the theoretical ionization potential 124417.491 cm^{-1} of Wolniewicz.[24] The vibronic matrices $\mathcal{J}$ and $\mathcal{C}$ were evaluated with a basis of 25 vibration−rotation channels v^+N^+ ($0 \le v^+ \le 24$), with $N^+ = 1$, 2, 3, or 4, whereby the vibrational wave functions were integrated from $R = 0.3$ to $R_{\text{max}} = 30$ au The higher solutions ($v^+ \ge 15$) are situated in the vibrational continuum of the ion core, where they act as quasibound ionization thresholds, which help to improve the convergence of the calculations. The quasibound levels have been calculated by enforcing the condition that $\chi_{v^+N^+}(R_{\text{max}}) = 0$. The ground-state vibrational wave function $\chi_{v'',N''}(R)$ was evaluated with the potential energy curve of Wolniewicz.[15]

For the purposes of comparison, we have also made calculations in the adiabatic approximation, following refs 25 and 26

but using the latest potential energy curves and adiabatic corrections for the $^1\Pi_u$ states.[14]

4. Results

Table 1 contains the results of our calculations concerning the $Q(1)$ transitions to the four lowest states of $^1\Pi_u$ symmetry of H_2. The table also compares the theoretical data with experimental line wavenumbers and intensities. Tables 2−5 of the Supporting Information provide a more complete account of our calculations of the $Q(N)$, $N = 1-4$ transitions, and they also present the comparisons with experimental and previous theoretical results. In the following, we discuss the various aspects in turn.

4.1. Bound State Energies. A large number of $Q(1)$ line frequencies have been measured experimentally for excitation energies up to 130000 cm^{-1} in ref 27 with an absolute accuracy between about 0.1 and 0.3 cm^{-1} (depending on the individual line measurements). These transitions involve principal quantum number values from $n = 3$ up to ∼40 and vibrational quantum numbers from $v = 0$ up to 11. Additional $Q(1)$ lines at higher energy have been assigned much more recently in ref 17, however, with an accuracy of only about 5 or 10 cm^{-1} (depending on the experimental run). Numerous $Q(N)$ lines have been reported by Takezawa.[28] These values are less accurate (∼1 cm^{-1}) than those of ref 27 since the pressure shift correction was not applied. Namioka[29] measured Q lines involving the 2pπC upper state in absorption, whereas Abgrall et al.[30,31] observed the emission of the $Q(N)$ transitions from the 2pπC and 3pπD upper states with an accuracy of typically 0.1 cm^{-1}. Some of the earlier observations mentioned above have been used for comparison with the first ab initio MQDT calculations carried out in the 1970s.[4] Most recently, numerous level positions belonging to the 2pπC, 3pπD, and 4pπD′ $^1\Pi_u^-$ states have been evaluated theoretically in the framework of a coupled-equations ab initio approach.[32] For our present purposes, we have used the following experimental data:

- $n = 2$, C and $n = 3$, D state; $Q(1)-Q(4)$; refs 30 and 31.
- $n \geq 4$, $Q(1)$ (except $n = 4-8$, $v = 0$); ref 27.
- $n \geq 4$, $Q(2)-Q(4)$; ref 28.
- $n = 4-8$, $v = 0$; ref 28.

Figure 2 displays the residuals observed − calculated obtained with the present MQDT approach (squares), those obtained in the adiabatic approximation (triangles), and those obtained in a nonadiabatic coupled-equations approach[32] (circles) for the $n = 2$, C and $n = 3$, D states. The superiority of the quantum defect method in the present application is obvious, in comparison with the adiabatic approximation, which neglects the nonadiabatic interactions, and also in comparison with the nonadiabatic coupled-equations calculations, where these exist.

Figure 3 displays the deviations observed − calculated for all $Q(1)-Q(4)$ transitions as functions of the total energy. Squares indicate the residuals obtained with MQDT, whereas circles represent the values corresponding to the subset of the $Q(N)$ lines for which coupled-equations calculations are available.[32] Except for the early MQDT results reported in refs 4 and 27 and the recent very high-n hyperfine calculations reported in refs 11 and 13, no nonadiabatic calculation of $Q(N)$ singlet transitions has, to our knowledge, ever been published for states with $n > 5$ or 6. Figure 3 shows that use of the MQDT techniques leads to an improvement of the agreement between experiment and theory. In particular, we see that several Q lines, which, when calculated in the adiabatic approximation, are situated several cm^{-1} away from the baseline of Figure 3 and therefore are perturbed, are correctly reproduced by MQDT. A few observed lines are not reproduced by MQDT. The most extreme examples are the 7pπ, $v = 1$ $Q(2)$ line near 124228 cm^{-1}, the 8pπ, $v = 0$ $Q(1)$ line near 122678 cm^{-1}, and the 5pπ, $v = 2$ $Q(3)$ line near 124060 cm^{-1}, for which the MQDT values deviate by +14, +7, and −8 cm^{-1} from the reported experimental value, respectively. We suspect that in these three cases, the experimental assignment may be in error. The remaining Q lines which are not reproduced by the theory to within their nominal error bar may well correspond in some cases to blended lines, which had not been recognized as such in the experimental work.

The overall improvement achieved by the MQDT is also borne out by the mean and the maximum values of the deviations of observed − calculated, which are collected in Table 6. It may be seen that the mean deviations of observed − calculated, which we obtain for the 2pπC and 3pπD states are about a factor of 2 lower than those in the previously best calculations. The main progress achieved by the present work, however, is that the calculations have been extended to high n values.

We mention finally that high Rydberg levels with $n = 55$ to 65 and with $v = 0$, having the same upper-state symmetry as the $Q(1)$ transitions (i.e., $N = N^+ = 1$, positive total parity), have been observed by millimeter wave spectroscopy with sub-MHz accuracy.[11] These high-precision data have also been interpreted by MQDT in an extended approach which accounts for hyperfine interaction. We have not included these levels in our analysis as they are outside of the scope of the present work.

4.2. Line Intensities. Figures 4 and 5 display the observed and calculated emission probabilities, plotted as functions of the vibrational quantum number v for the $n = 3-6$ and $7-10$ members of the $np\pi$ Q(1) series of H_2. For each vibrational progression associated with an electronic series member, the continuous line without symbols represents the probabilities calculated in the adiabatic approximation. Each of these lines exhibits a smooth Franck−Condon-type envelope whose maximum occurs for $v = 2$, as in the photoelectron spectrum of H_2. The overall decrease of the Franck−Condon envelope proportional to n^{-3} is also clearly visible along the sequence of plots; for instance, between $n = 3$ and 10, the Franck−Condon maximum drops by a factor of $(10/3)^3 = 37$, namely, from 7×10^7 s^{-1} to 0.2×10^7 s^{-1}, as expected on the basis of the Rydberg scaling rule.

This regularity is disrupted by the effects of nonadiabatic (vibronic) interactions (cf. the data points with filled and open squares in the figures). These perturbations are seen to become stronger as n increases, and they increase also with increasing vibrational excitation (compare, for instance, the inset in Figure 4a). This happens because the vibrational progressions become increasingly interleaved at higher energy, and therefore, more near coincidences of levels occur, which allows the channel couplings to become active. The quantum interferences yield both a strengthening and a weakening of transition intensities, and by and large, the lower n members of the $Q(1)$ series which are inherently strong become weakened by the vibronic coupling, whereas the opposite occurs in the higher n members, which are inherently rather weaker. Figure 6 is an analogous plot for the $Q(2)$ series, for which there is less experimental information.

The only database available at present that provides information on the intensities of the $Q(N)$ absorption lines of H_2 is the MOLAT astrophysical base published by Abgrall et al.,[33,34] which lists line intensities involving the C and D upper states only. The intensity data contained in this database result from

TABLE 1: Wavenumbers and Spontaneous Emission Coefficients to the $v'' = 0$ Level for the $Q(1)$ Absorption Transitions to $^1\Pi_u^-$ Rydberg States of H_2

v	state	wavenumber calc. present (cm^{-1})	obs.[a] − calc. present (cm^{-1})	obs. ref.	obs. − calc.; ref 32 (cm^{-1})	A(calc.) present (10^6 s^{-1})	A(calc.); ref 35 (10^6 s^{-1})	A(obs.)[a]; ref 17 (10^6 s^{-1})
0	2pπC	99033.01	−0.5 (0.1)	30	−0.2	154.72	155.70	
1	2pπ	101338.49	−0.4 (0.1)	30	−0.4	249.51	249.80	
2	2pπ	103509.98	−0.5 (0.1)	30	−0.8	251.24	250.00	
3	2pπ	105550.08	−0.4 (0.1)	30	−1.0	205.97	203.90	
4	2pπ	107460.46	−0.2 (0.1)	30	−1.2	151.85	149.60	
5	2pπ	109241.70	−0.0 (0.1)	30	−1.4	105.76	103.60	
6	2pπ	110892.91	0.4 (0.1)	30	−1.5	71.49	69.66	
7	2pπ	112411.77	0.6 (0.1)	30	−1.8	47.64	46.23	
8	2pπ	113793.90	0.9 (0.1)	30	−1.9	31.51	30.59	
9	2pπ	115032.50	1.1 (0.1)	30	−1.8	21.63	18.80	
10	2pπ	116117.15	0.4 (0.1)	30	−1.9	13.45	13.37	
11	2pπ	117031.96	−0.4 (0.1)	30	−1.6	8.53	8.68	
12	2pπ	117751.83	−1.6 (0.1)	30	−1.7	5.04	5.39	
13	2pπ	118233.59	−3.2 (0.1)	30	−4.0	2.37	2.64	
0	3pπD	112813.53	−0.4 (0.1)	31	−0.4	37.09	38.05	
1	3pπ	115036.42	−0.4 (0.1)	31	−0.6	64.55	67.22	
2	3pπ	117130.01	−0.5 (0.1)	31	−0.7	71.89	70.41	
3	3pπ	119098.02	−0.7 (0.1)	31	−1.0	63.51	60.42	
4	3pπ	120943.46	−0.7 (0.1)	31	−1.2	49.78	46.88	
5	3pπ	122668.51	−0.8 (0.1)	31	−1.4	36.28	34.13	
6	3pπ	124274.61	−0.7 (0.1)	31	−1.5	24.88	23.98	
7	3pπ	125760.44	−0.6 (0.1)	31	−1.6	23.25	16.53	
8	3pπ	127129.80	−0.7 (0.1)	31	−1.9	13.37	11.31	12.7 (0.9)
9	3pπ	128377.82	−0.4 (0.1)	31	−1.8	8.61	7.73	8.4 (0.6)
10	3pπ	129502.71	−0.3 (0.1)	31	−2.0	5.84	5.29	6.8 (0.5)
11	3pπ	130499.56	0.0 (0.1)	31	−2.0	4.95	3.63	5.5 (0.4)
12	3pπ	131365.79	0.1 (0.1)	31	−2.0	3.14	2.49	4.1 (0.4)
13	3pπ	132093.62	−0.2 (0.1)	31	−2.0	1.57	1.70	2.1 (0.15)
14	3pπ	132674.41	−1.2 (0.1)	31	−2.3	1.45	1.12	1.3 (0.2)
15	3pπ	133101.59	6.4 (5)	17	5.7	0.88	0.69	1.1 (0.13)
16	3pπ	133367.12	5.3 (5)	17	5.1	0.32	0.34	0.74 (0.11)
17	3pπ	133468.31	5.6 (5)	17	5.1	0.00	0.07	0.10 (0.01)
0	4pπD′	117775.64	−0.4 (1.0)	28	−0.7	13.93	14.54	
1	4pπ	119975.65	−0.1 (1.0)	28	−3.4	29.12	25.63	
2	4pπ	122050.78	−0.4 (1.0)	28	−3.5	32.98	29.01	
3	4pπ	124001.93	−0.1 (0.1)	27	−2.8	29.54	27.14	
4	4pπ	125834.24	−0.3 (0.1)	27	−2.3	15.60	15.45	11.0 (3.0)
5	4pπ	127543.33	0.5 (0.1)	27	3.2	16.98	14.56	13.0 (2.0)
6	4pπ	129140.36	−0.8 (0.1)	27	−2.8	12.20	10.93	11.3 (2.5)
7	4pπ	130622.28	3 (10)	36	1.3	7.22	6.70	5.9 (1.5)
8	4pπ	131987.82	6 (5)	36	5.7	5.41	5.60	5.4 (0.6)
9	4pπ	133240.20	6 (5)	36	6.9	3.16	3.49	4.0 (0.6)
10	4pπ	134379.91	7 (5)	36		1.16	2.55	1.2 (0.2)
11	4pπ	135384.53	1 (5)	36		2.19	1.83	1.6 (0.5)
12	4pπ	136282.75	6 (5)	36		1.68	1.32	2.3 (0.3)
13	4pπ	137055.32	9 (5)	36		0.83	0.93	0.84 (0.1)
14	4pπ	137679.17	1 (10)	36		1.45	0.65	1.18 (0.1)
15	4pπ	138199.74	7 (10)	36		0.41	0.43	0.42 (0.1)
16	4pπ	138555.12	5 (10)	36		0.52	0.25	0.67 (0.1)
17	4pπ	138776.83	3 (10)	36		0.15	0.14	0.12 (0.05)
0	5pπD″	120113.27	−0.2 (1.0)	28		3.88		
1	5pπ	122309.38	−0.6 (1.0)	28		9.21		
2	5pπ	124383.17	−0.9 (0.1)	27		4.02		3.6 (0.4)
3	5pπ	126319.12	−1.0 (0.1)	27		12.37		8.0 (0.6)
4	5pπ	128144.53	−2.4 (0.1)	27		9.94		5.3 (0.4)
5	5pπ	129851.66	1.5 (0.1)	27		7.40		5.5 (0.4)
6	5pπ	131443.05	3 (5)	17		5.57		3.77 (0.25)
7	5pπ	132920.57	9 (5)	17		3.95		8.9 (0.6)
8	5pπ	134281.80	9 (5)	17		3.08		3.7 (0.3)
9	5pπ	135534.97	3 (5)	17		1.70		1.8 (0.2)
10	5pπ	136674.43	8 (5)	17		1.54		2.3 (0.3)
11	5pπ	137714.71	−10 (10)	17		0.02		0.54 (0.06)
12	5pπ	138604.29	2 (10)	17		0.55		0.30 (0.04)
13	5pπ	139387.40				0.39		
14	5pπ	140044.72				0.28		
15	5pπ	140569.57				0.35		
16	5pπ	140957.90				0.14		

[a] Experimental uncertainty in parentheses.

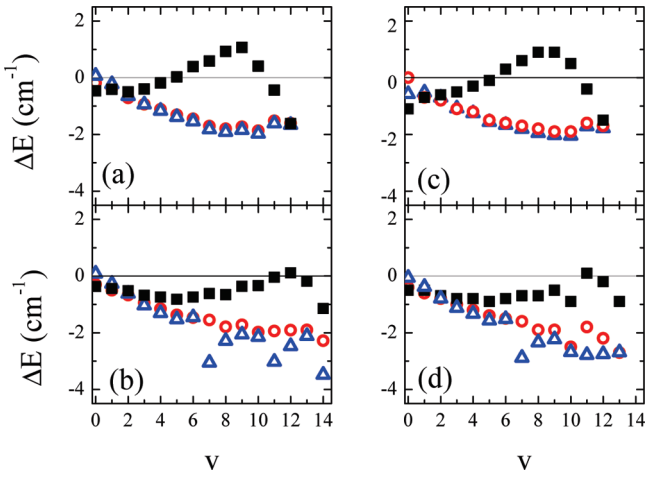

Figure 2. Deviations $\Delta E = E$(observed) $- E$(calculated), in cm^{-1}, of $Q(1)$ [(a) and (b)] and $Q(2)$ [(c) and (d)] transition energies involving the $2p\pi C$ [(a) and (c)] and $3p\pi D$ [(b) and (d)] upper states in H_2, plotted as functions of the upper-state vibrational quantum number v. Squares: present MQDT calculations. Circles: nonadiabatic (coupled equations) (Wolniewicz et al.[32]). Triangles: adiabatic approximation.

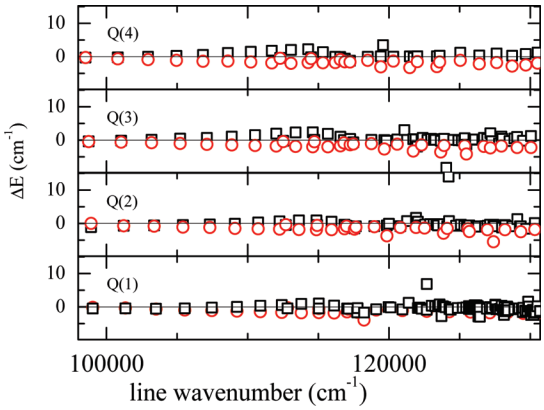

Figure 3. Deviations $\Delta E = E$(observed) $- E$(calculated), in cm^{-1}, of the $Q(1)$, $Q(2)$, $Q(3)$, and $Q(4)$ transitions (from bottom to top) in H_2, plotted as functions of their energy ($2p\pi C$ state omitted). Squares: present MQDT calculations. Circles: coupled-equations calculation.[32]

an empirical nonadiabatic coupled-equations calculation. This calculation takes account of the interaction between the $n = 2$, C and $n = 3$, D members of the $np\pi$ series and thus produces theoretical line intensities in which at least part of the nonadiabatic interactions have been included. It is instructive to compare our results with the Einstein A coefficients listed in this database.[35]

Figure 7 contains plots of calculated and/or observed Einstein A coefficients divided by those evaluated in the adiabatic approximation. It can be seen that in the case of the C upper state (Figure 7a and d), the nonadiabatic effects contribute less than 10% to the emission probabilities. The $Q(1)$ line corresponding to $v = 9$ in the upper state stands out since its intensity is perturbed by vibronic interaction with the $n = 3$, D ($v = 1$) member of the Rydberg series. Our calculation predicts a strengthening of the $Q(1)$ line associated with the C state, whereas the MOLAT data predict a weakening of the same line. We suspect that this disagreement is due to a sign inconsistency in the coupled-equations calculations. Panels b and e of Figure 7 compare the results for the $n = 3$, D upper state. The calculations reported in the MOLAT base do not include interactions with $n > 3$ members, and therefore, these values are, in essence, equivalent to the adiabatic approximation, as is indeed borne out by the data points shown in the figure.

Nonadiabatic perturbative calculations involving, in addition, the $n = 4$, D′ state have been published recently in ref 36. Up to $v = 8$ in the D′ upper-state progression, the perturbative nonadiabatic and the MQDT results are seen to be basically equivalent (Figure 7c and f), but for higher v, only the MQDT results take account of vibronic perturbations with higher $np\pi$ series members. Note how for Q transitions involving the $n = 4$, D′ upper state, the effects of vibronic interaction are much stronger and may modify the intensities up to a factor of 2 while the energy structure itself is hardly perturbed at all. The MOLAT base does not include the $n = 4$, D′ member of the $np\pi$ series.

We now turn to the comparison of our calculated line intensities with the absolute intensity measurements of ref 17. Figures 4−6 show that, with few exceptions, concerning mainly some of the weaker lines, MQDT accounts rather well, although not perfectly, for the intensity perturbations. There are, in all, 89 $Q(1)$ and $Q(2)$ lines whose intensities have been measured. We find that out of these, the intensities of (a) 19 lines, or 21%, are reproduced by MQDT but were not in the adiabatic approximation because they are notably affected by vibronic coupling; (b) 10 lines, or 11%, are improved by MQDT, without, however, agreeing with experiment to within the experimental error; (c) 51 lines, or 57%, are accounted for by the MQDT as well as by the adiabatic calculation because they are not subject to nonadiabatic interactions; (d) 5 lines, or 6%, were not accounted for by the adiabatic aproximation but are even in worse disagreement when MQDT is used, with a disagreement larger than 30%, which is the largest experimental uncertainty; and (e) 4 lines, or 4%, which were accounted for in the adiabatic approximation, are no longer accounted for by MQDT.

5. Discussion

Vibronic channel interactions of the type studied here are known to be dominated by $\Delta v = \pm 1$ couplings, leading, for instance, to the well-known "$\Delta v = -1$ propensity rule" in autoionization.[37] The detailed analysis of the present calculations shows that the intensity perturbations of the $Q(N)$ lines are, in many cases, more complex. Indeed, many of the most conspicuous intensity perturbations involve levels differing by $\Delta v = 2$ or 3. For instance, the $4p\pi$, $v = 4$ $Q(N)$ lines are weakened because their intensities are transferred toward the corresponding $3p\pi$, $v = 7$ lines, which are strengthened. Another example is afforded by $4p\pi$, $v = 14$, which is coupled to $5p\pi$, $v = 11$, that is, by a $\Delta v = 3$ interaction, with the result that (as the channel mixing coefficients B_k from eq 7 show) the vibronic wave functions are nearly 50:50 mixtures of the unperturbed channel components. As a consequence, the intensities of the $Q(N)$ lines leading up to $5p\pi$, $v = 11$ are nearly completely transferred to the corresponding lines involving $4p\pi$, $v = 14$.

Another complication which also emerges from our calculations is that, very often, the interactions are, in reality, multistate couplings. This fact is again borne out by the channel coupling coefficients B_k, but it also becomes apparent when one attempts to apply the familiar intensity sum rule. This rule states that the overall absorption intensity must remain unchanged when the upper-state level couplings are introduced in the calculation (in other words, there is an overall cancellation of constructive and destructive interferences). The intensity sum rule is of course verified by the present calculations, but in many cases, it turns out that one has to sum over more than two interacting upper levels in order to arrive at the required result. For instance, $4p\pi$, $v = 10$ is strongly coupled to $5p\pi$, $v = 8$. The channel mixing

TABLE 6: Deviations of Observed − Calculated of $Q(N)$ ($N = 1-4$) Transitions in $^1\Pi_u^-$ Rydberg States of H_2[a]

			MQDT[b]			coupled eqs.[c]			
	state	ref.	mean[d]	rms[e]	max.[f]	mean	rms	max.	num.[g]
$Q(1)$	2pπC	30	−0.04	0.67	−1.6	−1.17	1.32	1.9	13
	3pπD	31	−0.54	0.61	−1.2	−1.54	1.60	−2.3	15
	4pπD′	27, 28	−0.28	0.36	−0.8	−2.66	2.85	−3.9	7
	higher *n*pπ	27, 28	−0.49	1.16	6.8				122
$Q(2)$	2pπC	30	−0.14	0.74	−1.5	−1.35	1.46	−1.9	13
	3pπD	31	−0.63	0.69	−0.9	−1.55	1.68	−2.7	14
	4pπD′	28	−0.18	0.90	1.7	−2.80	3.18	−5.5	6
	higher *n*pπ	28	−0.39	0.76	1.7				58
$Q(3)$	2pπC	30	1.00	1.34	2.3	−1.36	1.45	2.0	13
	3pπD	31	0.46	0.71	1.6	−1.57	1.74	−3.4	14
	4pπD′	28	0.02	1.07	2.1	−2.84	3.00	−4.2	6
	higher *n*pπ	28	0.25	1.45	8.3				57
$Q(4)$	2pπC	30	0.74	1.19	2.2	−1.37	1.46	2.0	13
	3pπD	31	0.42	0.69	1.3	−1.58	1.63	−2.8	14
	4pπD′	28	−0.24	0.61	−1.2	−2.72	2.81	−3.3	4
	higher *n*pπ	28	0.53	1.08	3.5				33

[a] In cm^{-1}. [b] Present. [c] Reference 32. [d] Mean deviation of theoretical calculations. [e] Root-mean-square deviation of theoretical calculations. [f] Maximum deviation. [g] Number of levels used in calculating the mean and the rms error.

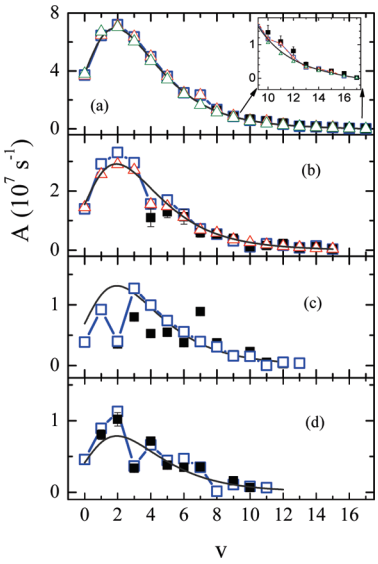

Figure 4. Einstein A coefficients for the $np\pi$ $Q(1)$ series ($v'' = 0$) in H_2 as functions of the upper-state vibrational quantum number v; (a) $n = 3$ (D state), (b) $n = 4$ (D′ state), (c) $n = 5$ (D″ state), and (d) $n = 6$. Filled squares with error bars: experimental values. Continuous lines without symbols: adiabatic approximation. Open squares: ab initio MQDT. Open triangles: nonadiabatic calculations. Note that the ordinate scales are different in (a), (b), (c), and (d).

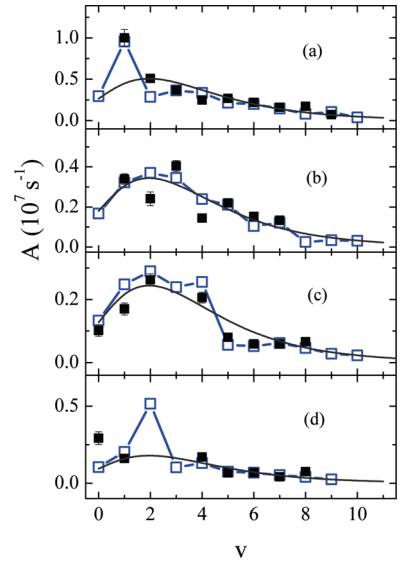

Figure 5. Einstein A coefficients for the $np\pi$ $Q(1)$ series ($v'' = 0$) in H_2 as functions of the upper-state vibrational quantum number v; (a) $n = 7$, (b) $n = 8$, (c) $n = 9$, and (d) $n = 10$. Filled squares with error bars: experimental values. Continuous lines without symbols: adiabatic approximation. Open squares: ab initio MQDT. Note that the ordinate scales are different in (a), (b), (c), and (d).

coefficients and the application of the intensity sum rule indicate, however, that 6pπ, $v = 7$ and 9pπ, $v = 6$ are involved in this interaction as well.

Multistate interactions occur more and more frequently at higher energies where the density of states increases. An extreme example is afforded by the $Q(1)$ transition leading to the 5pπ, $v = 2$ upper state, which is coupled to the corresponding 7pπ, $v = 1$ level as well as to the high $np\pi$, $v = 0$ series converging to the $v^+ = 0$, $N^+ = 1$ ionization threshold. This perturbation is illustrated in Figure 8. The figure demonstrates how MQDT allows us to assess the contributions of the various vibronic channels to the final line positions and intensities. The filled circles in the upper panel indicate the positions and intensities of 5pπ, $v = 2$ and 7pπ, $v = 1$ in the adiabatic approximation; the $v = 2$ line has more intensity due to the more favorable Franck−Condon factor and due to the lower n value. The filled triangles correspond to a calculation where only the $v^+ = 0$ and 1 channels have been included in the MQDT calculation; the vibronic $\Delta v^+ = 1$ interaction has increased the energy gap between the two lines and reversed their relative intensities. The lower panel is a zoom showing how inclusion of the $v^+ = 0$ channel dilutes the 7pπ, $v = 1$ line among the high-n ($n \approx 150-200$) $v^+ = 0$ Ry levels (open circles in the lower panel of the figure). Finally, inclusion of channels corresponding to $v^+ > 2$ shift the resulting "complex resonance" to higher energy, the main contributor to this shift being the 4pπ, $v = 3$ state, which lies at somewhat lower energy. Another example of a level which is embedded in a quasi-continuum is 7pπ, $v = 2$, $N = 1$, which is situated near the $n \approx 30$ member of the high-n $v = 1$ Ry series. According to our calculation, 7pπ, $v = 2$, $N = 1$ and 30pπ, $v = 1$, $N = 1$ are mixed and share the intensity associated with the former unperturbed level, but these lines were unresolved both in the experiment of ref 27 and in the intensity measurements of ref 17.

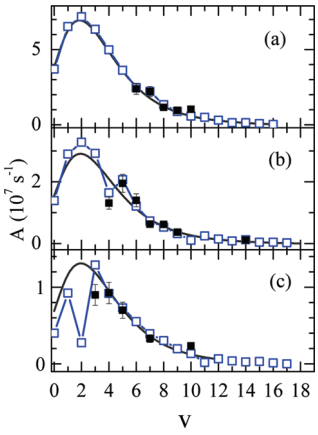

Figure 6. Einstein A coefficients for the $np\pi$ $Q(2)$ series ($v'' = 0$) in H_2 as functions of the upper-state vibrational quantum number v; (a) $n = 3$ (D state), (b) $n = 4$ (D′ state), and (c) $n = 5$ (D″ state). Filled squares with error bars: experimental values. Continuous lines without symbols: adiabatic approximation. Open squares: ab initio MQDT. Note that the ordinate scales are different in (a), (b), and (c).

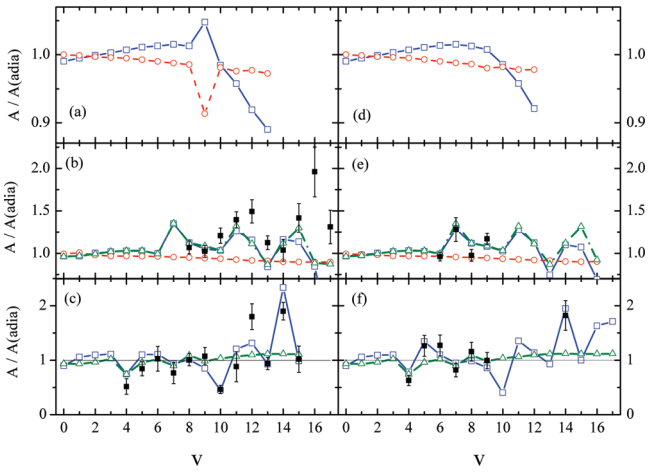

Figure 7. Ratios of nonadiabatic or observed to adiabatic Einstein A coefficients for the $np\pi$ $Q(1)$ ($v'' = 0$) [(a), (b), (c)] and $Q(2)$ lines ($v'' = 0$) [(d), (e), (f)] in H_2 as functions of the upper-state vibrational quantum number v. Open circles: MOLAT database/adiabatic. Open squares: MQDT/adiabatic. Filled squares with error bars: experimental/adiabatic. Triangles: nonadiabatic/adiabatic (ref 36); (a and d) $n = 2$ (C state), (b and e) $n = 3$ (D state), (c and f) $n = 4$ (D′ state).

A somewhat counterintuitive aspect of the present calculations is that they show that strong interactions do not necessarily produce strong intensity perturbations, while, on the other hand, rather weak channel mixings may lead to conspicuous intensity perturbations. For example, 4pπ, $v = 5$ is mixed strongly with 6pπ, $v = 3$ and weakly with 10pπ, $v = 2$, which has ~4% weight in the wave function. Yet, this perturbation affects the A value of 10pπ, $v = 2$ strongly, but has only a limited effect on 4pπ, $v = 5$.

6. Conclusion

We have shown that vibronic interactions among the $^1\Pi_u^-$ excited states of H_2, while only weakly affecting the energy level positions, have a major effect on the intensitites of the $Q(N)$ absorption lines. Ab initio multichannel quantum defect theory proves to be an adequate theoretical tool for the description of the absolute intensities of these transitions, and it remains competitive with regard to the coupled channels approach inasmuch as energy level positions are concerned.

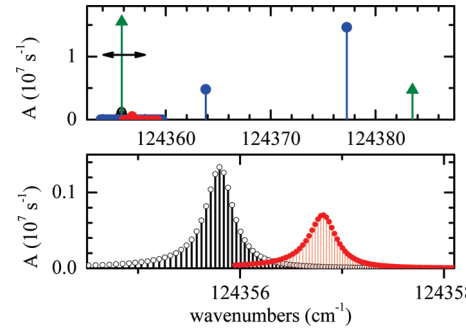

Figure 8. $Q(1)$ Einstein A coefficients ($v'' = 0$) near the $v^+ = 0$, $N^+ = 1$ ionization threshold of H_2. (Upper panel) Filled circles: positions and intensities of 5pπ, $v = 2$ and 7pπ, $v = 1$ calculated in the adiabatic approximation. Filled triangles: positions and intensities of 5pπ, $v = 2$ and 7pπ, $v = 1$ calculated by MQDT including the $v^+ = 1$ and 2 channels only. (Lower panel) Zoom of the region near 7pπ, $v = 1$ (indicated by a horizontal arrow in the upper panel). Open circles: result of the MQDT calculation when the $v^+ = 0$ channel is included in addition to $v^+ = 1$ and 2. Filled circles: result of the converged MQDT calculation including $0 \le v^+ \le 24$.

A comment on some of the comparative advantages and disadvantages of the nonadiabatic MQDT and coupled equations approaches may be in order here. The strength of MQDT is that multichannel quantum defect theory accounts, albeit in an approximate manner, for nonadiabatic interactions of all np $^1\Pi_u^-$ excited states, including those belonging to the electronic continuum. By contrast, the coupled equations approach of ref 32 included interactions only within a restricted manifold of states, namely, the 2pπ, 3pπ, 4pπ, and 4fπ states. The electronic interaction coupling functions involving the p states with $n = 2-4$ were calculated in ref 32 essentially exactly, whereas MQDT implicitly assumes approximate values for these interaction matrix elements. For instance, in the present application, it is assumed that the angular dependence of the Rydberg wave function has pure $l = 1$, that is, p, character for all R values. The f channels are not included explicitly in our treatment, and therefore, any l mixing between the $l = 1$ and 3 channels is disregarded. However, the restriction of our treatment to nominal $l = 1$ channels concerns only the nonadiabatic interactions, which themselves are relatively small in the excited levels studied here. Figures 2 and 3 and Table 6 demonstrate that, despite these shortcomings, the balance ultimately leans in favor of the MQDT approach.

The present work constitutes a first step toward a full theoretical description of the absorption spectrum of H_2, including absolute line intensities up to the H($n = 3$) + H(1s) and H($n = 4$) + H(1s) dissociation limits. In order to achieve this goal, several additional features will have to be introduced into the MQDT approach used here. Beyond including rotational channel interactions, which are not relevant for the Q transitions studied here, one will have to include l mixing interactions such as the p−f mixing just mentioned. The restriction of our treatment to nominal $l = 1$ channels obviously must eventually become inadequate as the energy increases as the range of vibrational motion extends to larger R values and the molecule departs more and more from spherical symmetry. The clamped nuclei ab initio calculations of the Wolniewicz group[14] indicate indeed that a rapid change of character of the electronic $^1\Pi_u$ wave functions occurs near $R = 10$ au, which is due to avoided crossings between Born−Oppenheimer curves of predominant p and f character, respectively. It produces the cusp-like behavior of the dipole transition functions $d^{(i)}(R)$ seen in Figure 1 at this R value. This type of interaction affects the $^1\Sigma_u$ channels much

more strongly than the $^1\Pi_u$ channels. These electronic interactions produce double-minimum potential energy curves of the type familiar from the $^1\Sigma_g^+$ manifold of states, which will need to be taken into account properly and whose effects in the case of ungerade channels at higher energy are not yet well understood.

Acknowledgment. Ch. J. thanks the Miescher Foundation (Basel, Switzerland) for partial support.

Supporting Information Available: Tables 2−5: complete list of calculated line frequencies and intensities. Comparison with experimental and other theoretical data. This material is available free of charge via the Internet at http://pubs.acs.org.

References and Notes

(1) Seaton, M. J. *Rep. Prog. Phys.* **1983**, *46*, 167 (reprinted in ref 2).
(2) *Molecular Applications of Quantum Defect Theory*; Jungen, Ch., Ed.; The Institute of Physics: Bristol, U.K., 1996.
(3) Fano, U. *Phys. Rev. A* **1970**, *2*, 353 (reprinted in ref 2).
(4) Jungen, Ch.; Atabek, O. *J. Chem. Phys.* **1977**, *66*, 5584 (reprinted in ref 2).
(5) Ross, S. Ch.; Jungen, Ch. *Phys. Rev. A* **1994**, *49*, 4364 (reprinted in ref 2).
(6) Yu, S.; Dressler, K. *J. Chem. Phys.* **1994**, *101*, 7692.
(7) Jungen, Ch.; Dill, D. *J. Chem. Phys.* **1980**, *73*, 3338.
(8) Jungen, Ch.; Dabrowski, I.; Herzberg, G.; Vervloet, M. *J. Chem. Phys.* **1990**, *93*, 2289.
(9) Fredin, S.; Gauyacq, D.; Horani, M.; Jungen, Ch.; Lefevre, G. *Mol. Phys.* **1987**, *60*, 825.
(10) Field, R. W.; Gittins, C. M.; Harris, N. A.; Jungen, Ch. *J. Chem. Phys.* **2005**, *122*, 184314.
(11) Osterwalder, A.; Wüest, A.; Merkt, F.; Jungen, Ch. *J. Chem. Phys.* **2004**, *121*, 11810.
(12) Cruse, H. A.; Jungen, Ch.; Merkt, F. *Phys. Rev. A* **2008**, *77*, 042502.
(13) Wörner, H. J.; Mollet, S.; Jungen, Ch.; Merkt, F. *Phys. Rev. A* **2007**, *75*, 062511.
(14) Wolniewicz, L.; Staszewska, G. *J. Mol. Spectrosc.* **2003**, *220*, 45.
(15) Wolniewicz, L. *J. Chem. Phys.* **1993**, *99*, 1851.
(16) Index of Publications; http://www.fizyka.umk.pl/ftp/publications/ifiz/luwo/.
(17) Glass-Maujean, M.; Klumpp, S.; Werner, L.; Ehresmann, A.; Schmoranzer, H. *Mol. Phys.* **2007**, *105*, 1535.
(18) Greene, C. H.; Jungen, Ch. *Adv. At. Mol. Phys.* **1985**, *21*, 51.
(19) Du, N. Y.; Greene, C. H. *J. Chem. Phys.* **1986**, *85*, 5430.
(20) Lee, C. M.; Lu, K. T. *Phys. Rev.* **1973**, *A8*, 1241.
(21) Wind, H. *J. Chem. Phys.* **1965**, *42*, 2371.
(22) (a) Bishop, D. M.; Wetmore, R. W. *Mol. Phys.* **1973**, *26*, 145. (b) Bishop, D. M.; Wetmore, R. W. *Mol. Phys.* **1974**, *27*, 279.
(23) Wolniewicz, L.; Orlikowski, T. *Mol. Phys.* **1991**, *74*, 103.
(24) Wolniewicz, L. *J. Chem. Phys.* **1995**, *103*, 1792.
(25) Allison, A. C.; Dalgarno, A. *At. Data Nucl. Data Tables* **1970**, *1*, 289.
(26) Glass-Maujean, M. *At. Data Nucl. Data Tables* **1984**, *30*, 301.
(27) Herzberg, G.; Jungen, Ch. *J. Mol. Spectrosc.* **1972**, *41*, 425.
(28) Takezawa, S. *J. Chem. Phys.* **1970**, *52*, 2575–5793.
(29) (a) Namioka, T. *J. Chem. Phys.* **1964**, *40*, 3154. (b) Namioka, T. *J. Chem. Phys.* **1964**, *41*, 2141.
(30) Abgrall, H.; Roueff, E.; Launay, F.; Roncin, J. Y.; Subtil, J. L. *J. Mol. Spectrosc.* **1993**, *157*, 512.
(31) Abgrall, H.; Roueff, E.; Launay, F.; Roncin, J. Y. *Can. J. Phys.* **1994**, *72*, 856.
(32) Wolniewicz, L.; Orlikowski, T.; Staszewska, G. *J. Mol. Spectrosc.* **2006**, *238*, 118.
(33) Abgrall, H.; Roueff, E.; Launay, F.; Roncin, J. Y.; Subtil, J. L. *Astron. Astrophys. Suppl.* **1993**, *101*, 273.
(34) Abgrall, H.; Roueff, E.; Launay, F.; Roncin, J. Y.; Subtil, J. L. *Astron. Astrophys. Suppl.* **1993**, *101*, 323.
(35) MOLAT, Atomic and Molecular Data; http://molat.obspm.fr.
(36) Glass-Maujean, M., S.; Klumpp, Werner, L.; Ehresmann, A.; Schmoranzer, H. *J. Chem. Phys.* **2008**, *128*, 94312.
(37) Dehmer, P. M.; Chupka, W. A. *J. Chem. Phys.* **1976**, *65*, 2243.

JP902846C